ELSEVIER

Physica C 383 (2003) 365–373

PHYSICA C

www.elsevier.com/locate/physc

The resistive transition of $(Hg_{0.85}Re_{0.15})(Ba_{1-y}Sr_y)_2Ca_2Cu_3O_{8+\delta}$ superconducting polycrystals

A.J. Batista-Leyva [a,b,*], M.T.D. Orlando [c], L. Rivero [a], R. Cobas [a], E. Altshuler [a]

[a] *Superconductivity Laboratory, IMRE-Physics Faculty, University of Havana, 10400 Havana, Cuba*
[b] *Department of Physics, University of Holguín, Holguín 80100, Cuba*
[c] *Department of Physics, Universidade Federal do Espírito Santo, Vitória-ES 29060-600, Brazil*

Received 17 December 2001; received in revised form 28 February 2002; accepted 19 April 2002

Abstract

The resistive transition of $(Hg_{0.85}Re_{0.15})(Ba_{1-y}Sr_y)_2Ca_2Cu_3O_{8+\delta}$ superconducting polycrystals, with $y = 0.00$, 0.17, 0.20 and 0.28 has been experimentally studied at different magnetic fields ($\leqslant 500$ Oe), being the Arrhenius plot characterized by two linear regions with different slope in the resistive tail. The crossover temperature between them depends on the Sr content. The dependence of the intergranular pinning energy with the magnetic field, for both regions, follows a power law, being the exponent dependent on the Sr content in a non-linear way. The intergranular irreversibility line benefits from the Sr doping, associated with the improvement of the transport properties (even in the normal state) with the increment of Sr. The contribution of fluctuations to the conductivity is calculated from the measurement of resistivity in the interval of 130–300 K, and the interlayer coupling energy is obtained. From these calculations, an estimation has been made of the interlayer distance, finding an increment with Sr content. Our study suggests that the Sr can improve the performance of Hg-based HT_c polycrystals for transport applications, which are basically determined by intergranular properties.

Keywords: Hg-1223; Irreversibility line; HT_cs; Polycrystals; Pinning energy; Ba–Sr substitution

1. Introduction

Since the discovery of the Hg-based high T_c superconductor (HT_c) family by Putilin et al. in 1993 [1], an intense research effort has been devoted to understand its properties. Among these compounds, with general formula $HgBa_2Ca_{n-1}Cu_nO_z$ ($n = 1, 2, 3 \ldots$), the one having $n = 3$ (Hg-1223) is the most attractive, due to its very high critical temperature (135 K) [2], and low anisotropy. Nevertheless, this compound has serious disadvantages for practical applications, because of its chemical instability, its relatively weak pinning, and a delicate sintering process (complicated by the toxicity of Hg). It has been established that chemical doping improves these drawbacks. Shimoyama et al. [3] and Kishio et al. [4] showed the benefits of doping with rhenium (compound (HgRe)-1223) regarding the rising of the

* Corresponding author. Address: Superconductivity Laboratory, IMRE-Physics Faculty, University of Havana, 10400 Havana, Cuba.
E-mail addresses: alfobatista@yahoo.com, abatista@uho.hlg.edu.cu (A.J. Batista-Leyva).

0921-4534/02/$ - see front matter
PII: S0921-4534(02)01346-1

irreversibility line. The development of new preparation routes [5] is a method for obtaining, in a faster way, better superconducting compounds. The preparation of compounds in which Ba is partially substituted by Sr (with general formula $(Hg_{1-x}Re_x)(Ba_{1-y}Sr_y)_2Ca_2Cu_3O_{8+\delta}$), gave rise to a group of superconducting materials with lower anisotropy, reflected in the improvement of irreversibility line and enhanced chemical stability [6]. These effects are supposed to result from the application of the so-called "chemical pressure", through the decrease of c-axis due to the substitution of Ba^{2+} by an ion of smaller ionic radius. Yamaura et al. [7] succeeded in obtaining the Ba free compound, which seems to be overdoped as prepared, reaching a critical temperature of 120 K after an annealing, with high stability in air at room temperature.

The practical applications of superconducting ceramic materials are restricted by the peculiar field and temperature behavior of the weak links between grains. No matter how good properties the grains have, the transport critical current will depend on the conductivity of the junctions between grains. This weak link network provokes that dissipation eventually appears at temperatures (or fields) lower than the intragranular critical temperature (field) T_{c0} (H_{c1g}). The intergranular irreversibility line may be defined as the locus (H_{irr}, T) at which the transport critical current density is zero. An estimation of this line can be given by the locus (H, T_z), being T_z the zero resistance critical temperature at field H, i.e., the temperature at which dissipation starts, considering an appropriate voltage criterion.

In the present paper, a study of the resistive transition of the polycrystalline compound $(Hg_{0.85}Re_{0.15})(Ba_{1-y}Sr_y)_2Ca_2Cu_3O_{8+\delta}$ with $y = 0.00$, 0.17, 0.20 and 0.28 is performed, in order to understand the influence of Sr on transport properties of this Hg based HT_c. The resistivity vs. temperature curves, at different applied magnetic fields, are recorded, from which the intergranular pinning energy and its dependence with magnetic field are obtained. The intergranular irreversibility temperature is estimated based on the criterion stated above. From the curves recorded up to 300 K, the interlayer coupling energy has been determined.

2. Experimental

2.1. Preparation technique

The formation of the multiphase ceramic precursor begins with the mixture of stoichiometric amounts of $Ba_2Ca_2Cu_3O_x$ (99.0%, PRAXAIR), ReO_2 and $Sr_2Ca_2Cu_3O_x$ (synthesized from CuO, $SrCO_3$ and $CaCO_3$ at 850 and 930 °C under O_2 with intermediate grindings) in powder form. They were homogenized in an agate mortar and pelletized with an uniaxial pressure of 0.5 GPa. The pellet obtained was annealed at 850 °C in a flow of oxygen during 15 h. Subsequently, it was crushed and compacted again before being annealed a second time at a higher temperature (930 °C) during 15 h in a flow of oxygen. The obtained precursor material was then submitted to a heat treatment at 930 °C during 12 h in a flow of a gas mixture of argon (99.95%) and oxygen (99.5%) maintained at 1 bar. The oxygen pressure p_{O_2} used during this last treatment was 0.10 bar. The synthesis of the ceramic superconductor $Hg_{0.85}Re_{0.15}(Ba_{1-y}Sr_y)_2Ca_2Cu_3O_{8+\delta}$ was carried out by means of the sealed quartz tube technique. The multiphase precursor material previously described was blended with HgO in stoichiometric proportions. A ramp of 300 °C/h up to 700 °C was applied, followed by one of 120 °C/h up to 835 °C where the temperature stayed for 10 h. Subsequently, the sample was cooled down to room temperature at a rate of 120 °C/h. The quartz tube filling factor, used in the synthesis of these samples, $f \approx 0.60$–0.70 g/cm^3, was a suitable value to obtain a single-phase superconducting (HgRe)-1223 compound. During the process, the samples were wrapped with gold foil.

The compounds with $y = 0.00$, 0.17, 0.20 and 0.28 were synthesized, and will be named below Sr00, Sr17, Sr20 and Sr28, respectively. These doping levels are those given by EDX analysis on the final products. Nominal values were 0.00, 0.15, 0.20 and 0.28, respectively.

2.2. Measurements

R vs. T measurements were performed in an automatic installation, described elsewhere [8].

The measurement procedure and data processing was similar to that of Ref. [9]. The 500 point R vs. T curves were recorded at a constant sweep rate of 2 K/min from 110 to 140 K, being the temperature controlled by a temperature controller Lake Shore 330, with a resolution of ± 0.1 K. A magnetic field, in the interval 0–500 Oe, was generated by a long solenoid, and applied perpendicular to the transport current of approximately 1.50 mA rms, small enough to neglect self-field effects. The criterion for the onset critical temperature (T_{c0}) was the maximum of the derivative of the R vs. T curve, and for T_z we used the voltage criterium $\ln(\rho_0/\rho_z) = 4$, $\rho_z = \rho(T_z)$, being ρ_0 the resistivity at the temperature T_0 where the curves measured for different fields splitted (see Fig. 2).

A detailed measurement of the resistivity was performed in the interval 120–300 K, at 1 K/min, with an uncertainty better than 0.1 K.

SEM micrographs were obtained in a LEICA Cambridge S440I electron microscope. EDX signal was recorded by an Oxford link microanalysis system in order to obtain a quantitative analysis. XRD was performed in a diffractometer Rigaku, model D-MAX 2000.

3. Results and discussion

3.1. Results

EDX results are shown in Table 1. In all cases small amounts of Si and C were detected as contaminants, although no analysis of phase purity was performed. X ray diffraction shows a shrinking of c-axis with the increment of Sr. For the undoped sample $c = 15.697$ Å, lowering its value to 15.632 Å (Sr17), 15.625 Å (Sr20) and 15.600 Å (Sr28). Regarding grain morphology, SEM images, shown in Fig. 1, showed that the increment of the Sr content increases the grain size, and changes dramatically its shape: while Sr17 (Fig. 1(a)) sample has grains of relatively small size (~5 μm) and irregular shape ("smeared" grains), for Sr20 (Fig. 1(b)) the grain size is bigger (~9 μm) and the grains are more regular, appearing some plate like grains. Regarding the Sr28 sample (Fig. 1(c)), larger grains are found (~20 μm), and the large grain population is mainly plate like, with regions in which a large number of grains are stacked together; the small round grains seam to be inclusions of $CaHgO_2$. The microstructure of the Sr00 sample (not shown here) is similar to that reported in Ref. [10] and consists in a combination of piled up plate like grains and grains of thicker cross section (~10 μm) with inclusions of $CaHgO_2$ and $Ba_2Cu_3O_5$; all these features are common in HgRe-1223 ceramics.

In Fig. 2, the Arrhenius plot [$\log(\rho/\rho_0)$ vs. $1/T$] for Sr20 at some selected fields is shown. As usual in ceramic superconductors, a relatively low magnetic field provokes the presence of a "resistive tail", related with the properties of the intergranular region [11]. In contrast with YBCO and BSCCO, for whom the tails in the Arrhenius plot are markedly non-linear [9], the plot for Sr substituted ceramic is quite linear, similar to that of (HgRe)-1223, reported in Ref. [9]. However, we should note that, as indicated by the solid lines depicted for $H = 0$ and $H = 500$ Oe, two linear regimes can be identified in the resistive tail; a crossover point between both regimes (T_{cs}) is indicated. We will refer to these regimes as "low temperature" regarding the one between the end of

Table 1
Sample composition (atomic), obtained from EDX

Sample	Hg	Re	Ba	Sr	Ca	Cu
Sr00, intragrain	0.85	0.15	2.10	–	2.20	3.10
Sr17, intragrain	0.85	0.15	0.84	0.17	1.97	3.12
Sr17, intergrain	0.85	0.11	0.79	0.16	2.15	2.91
Sr20, intragrain	0.85	0.16	0.85	0.20	1.83	3.15
Sr20, intergrain	0.85	0.12	0.72	0.15	1.85	2.75
Sr28, intragrain	0.85	0.14	0.74	0.28	1.75	3.02
Sr28, intergrain	0.85	0.10	0.64	0.29	2.15	3.03

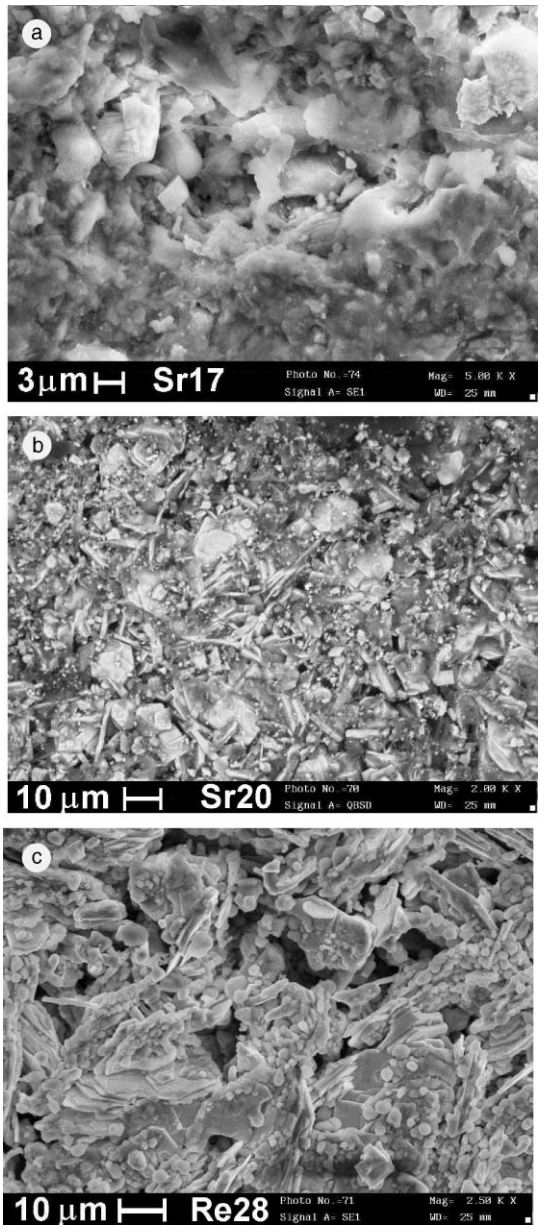

Fig. 1. SEM images of the Sr doped samples: (a) Sr17 sample, (b) Sr20 sample and (c) Sr28 sample.

the curve and the crossover point, and "high temperature" in the region between the crossover point and the point of splitting of the curves. This behavior repeats for all samples (except Sr00, for which the resistive tales are straight), and the slopes of the two parts are obtained through linear

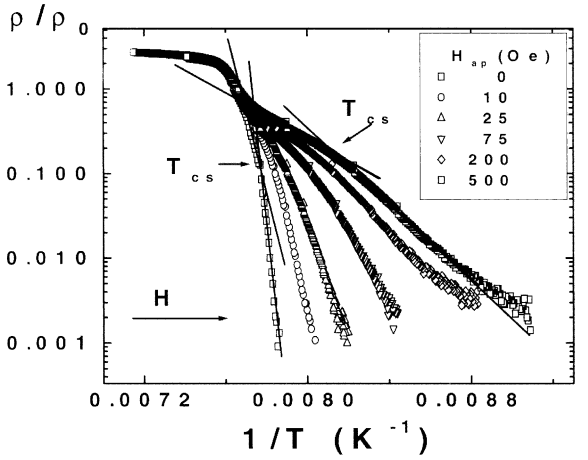

Fig. 2. Arrhenius plot for Sr20 at some selected fields. The two linear sections are highlighted for $H = 0$ and $H = 500$ Oe.

fit of a $\ln(\rho/\rho_0)$ vs. $1/T$ plot. It is important to state that for all the fitted curves, the regression coefficient is always better than 0.97, and the error in the slope is $<1\%$.

In the same spirit of Ref. [9], we assume that

$$\rho = \rho_0 \exp\left\{ -\frac{U_p(H,T)}{k_B T} \right\} \tag{1}$$

where k_B is Boltzmann constant, and the pinning energy can be expressed as

$$U_p(H,T) = U(H)\left(1 - \frac{T}{T_0}\right)^{\alpha} \tag{2}$$

and

$$\rho(T_0) = \rho_0 \tag{3}$$

The fact that the Arrhenius plot is linear on each regime means that the exponent $\alpha = 1$ (at least in this low magnetic field–high temperature window), in agreement with the findings of Ref. [9], obtained for a HgRe-1223 ceramic. The crossover temperature, T_{cs} is determined as the temperature at the point where the two lines intersect (Fig. 2).

The pinning energy can be obtained from the slope of the Arrhenius plot, as:

$$\ln\frac{\rho}{\rho_0} = \left[-\frac{U(H)}{k_B} \right]\frac{1}{T} + \frac{U(H)}{k_B T_0} \tag{4}$$

The dependence of the pinning energy (obtained from the above-mentioned slope) with magnetic field is sketched in Fig. 3. The dependence for the low temperature part of the resistive tail (U_1) is represented in Fig. 3(a), and that for the high temperature part (U_2) is shown in Fig. 3(b). In all cases the functional relation between the pinning energy and the applied magnetic field can be fitted to a power law:

$$U(H) = AH^{-n} \tag{5}$$

In the legends of Fig. 3, in parentheses, the n values resulting for different Sr contents are summarized.

The curves T_z vs. H_{irr} for all Sr content are represented in Fig. 4(a). The behavior of Sr00 sample is similar to that of Ref. [9], i.e., a sample with a Re proportion of about 0.18 with no Sr substitution. The temperature dependence of the

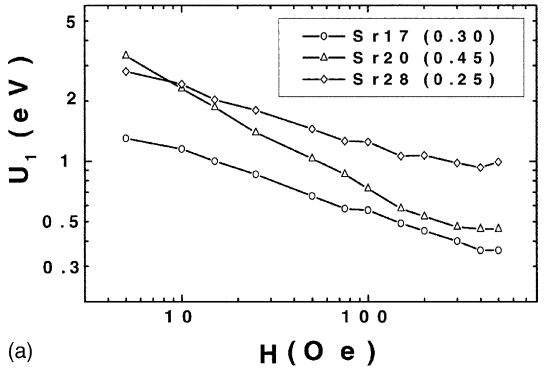

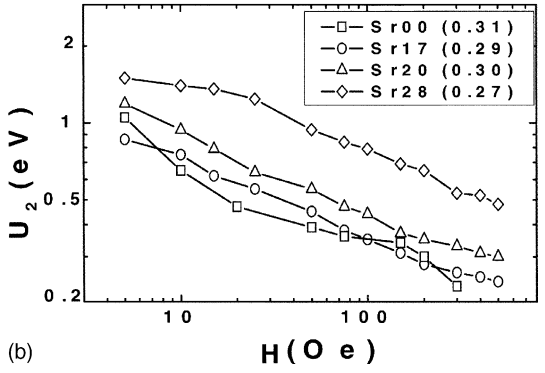

Fig. 3. Field dependence of the pinning energy for the (a) low and (b) high temperature part of the resistive tail for different Sr contents. n values (from $U(H) = AH^{-n}$) are shown in parentheses. The lines are guides to the eye.

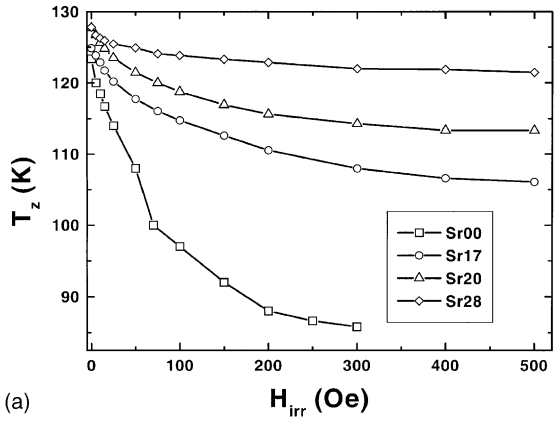

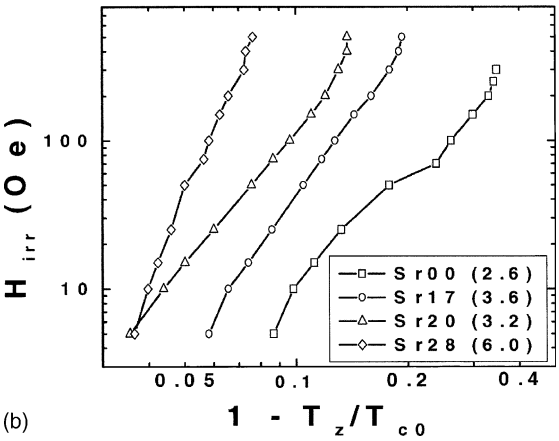

Fig. 4. (a) Intergranular irreversibility line (T_z, H_{irr}) for different Sr contents. The lines are guides to the eye. (b) Intergranular irreversibility line H_{irr} vs. $(1 - T_z/T_{c0})$ for different Sr content, in parentheses the values of slope. The lines are guides to the eye.

irreversibility field, described as a power law $(1 - T_z/T_{c0})^n$ is shown in Fig. 4(b). In the legend, in parentheses, the exponent of the power law is also shown. It is interesting that the line (H, T_{cs}), being T_{cs} the crossover temperature between the two different dissipation regimes, also follows the general behavior of the irreversibility line.

The resistive transition curves for all the samples, measured in the temperature range of 120–300 K, at 1 K/min, are shown in Fig. 5. From these curves, the values of the fitting parameters in $\rho = a + bT$ are obtained for the normal state, and the values are shown in Table 2, together with T_{c0} and T_z.

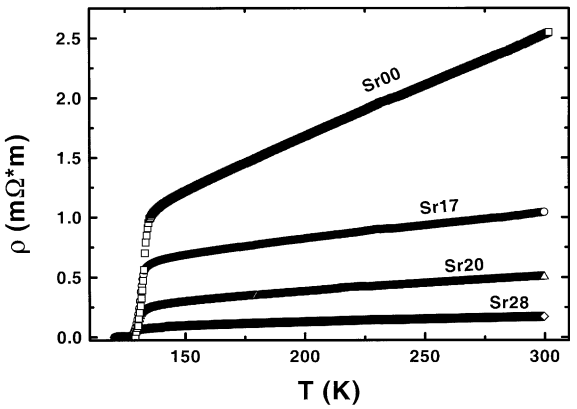

Fig. 5. R vs. T between 120 and 300 K for different Sr contents.

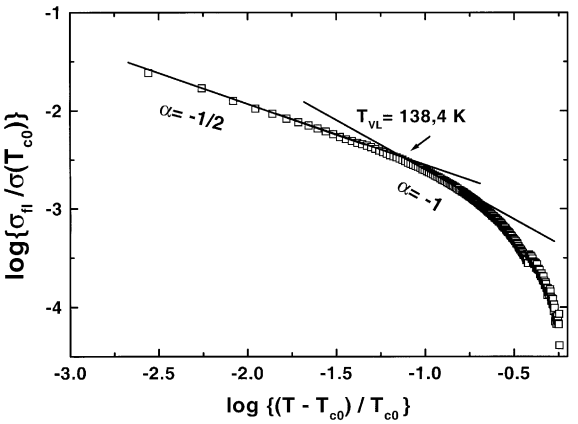

Fig. 6. $\log[\sigma_{fl}/\sigma(T_{c0})]$ vs. $(T - T_{c0})/T_{c0}$ for $y = 0.20$. The "Varlamov–Livanov" temperature is indicated (see text).

Fig. 6 represents the dependence of $\log[\sigma_{fl}/\sigma(T_{c0})]$ vs. $(T - T_{c0})/T_{c0}$ ($\sigma_{fl} = \sigma - \sigma_n$) for $y = 0.20$, being σ_n the normal state conductivity of the sample obtained by fitting the σ vs. T data to

$$\sigma_n = \frac{1}{a + bT} \tag{6}$$

in the interval (150–300 K). The term $(\sigma - \sigma_n)$ gives an estimate of the fluctuation contribution to conductivity [12,13] in the temperature range slightly above the onset critical temperature. In this figure, the crossover point between the slope of -1 to $-1/2$, at the so-called Varlamov–Livanov temperature (T_{VL}), is related with the onset critical temperature by [14]:

$$T_{VL} = T_{c0} + T_{c0}\delta_{VL}^2 \tag{7}$$

and

$$\delta_{VL} = K\frac{U_c}{k_B T_{c0}} \tag{8}$$

being U_c the interlayer coupling energy, inversely proportional to the interlayer distance, and K a known constant. The last column of Table 2 shows the values of this energy for different Sr contents.

3.2. Discussion

As was stated before, R vs. T curves have two regimes of dissipation. In the legends of Fig. 3(a) and (b) the value of the exponent n in the power law (Eq. (5)), for different Sr substitution, are shown in parentheses. As can be seen, n depends on the Sr content strongly for the low temperature part. The pinning energy for most of the applied fields, grows with Sr contents and, with the exception of the intermediate concentration (Sr20), the slope decreases. This two facts imply, firstly, that the slope in the Arrhenius plot for the low temperature part, at a given field, becomes steeper when the amount of Sr grows, and, secondly, *that Sr helps in creating an intergranular region less sensitive to the applied magnetic field*. As was stated before, the exception is Sr20: for this concentra-

Table 2
Dependence of some selected parameters with Sr content

Sr content	T_{c0} (K)	$T_z(H = 0)$ (K)	a (mΩ m)	b (mΩ m K^{-1})	U_c (meV)
0.00	132.9	123.4	0.0432	0.00860	4.2
0.17	131.3	124.9	0.0974	0.00229	3.8
0.20	130.3	127.7	0.0360	0.00138	3.5
0.28	128.7	127.8	0.0311	0.00048	3.2

tion, a more "penetrable" intergranular region is created. The reason could be related with the fact that, for this compound, the stoichiometry of intergranular region is altered, when compared with the nominal (and intragranular) one, as is revealed by EDX, while Sr17 and Sr28 have approximately stoichiometric concentrations (see Table 1). This worsening of the superconducting quality in the intergranular region is consistent with the stronger field dependence of the pinning energy observed for Sr20 in Fig. 3(a): at low fields, the pinning energy of Sr20 sample is high (even higher than that of Sr28), but when the magnetic induction grows, the current carrying capabilities of the weak links strongly decrease, lowering the pinning energy of the Josephson vortexes. It is also remarkable in Fig. 3(b) that the variations in the slope, for the high temperature part, are small, being those of the doped samples almost equal to that of the undoped. The increment in pinning energy is also smaller for U_2 than for U_1.

This two regime behavior has also been found in a Re doped sample (without Sr) that was irradiated with neutrons, with a fluence of 10^{22} m^{-2} [15]. That sample showed almost the same slope in the high temperature part ($n = 0.32$), although the slope of the low temperature section ($n = 0.74$) is greater than that found in the samples examined here.

A possible interpretation of this two-regime behavior can be ascribed to the existence of two population of weak links, one of them determined by the presence of Sr in the intergranular region, as well as in the grain border, or, in the case of Ref. [15], by the effect of irradiation (that must introduce defects in the intergranular region, producing a change in the links between grains). It is important to note that, according to Eq. (4) and Fig. 2, the parameter T_0 for the population ascribed to the low temperature part must be smaller than that for the other population.

In Fig. 4(a), the increase of Sr content shows a pronounced effect over the irreversibility temperature: for the Sr free sample, not only the absolute values of irreversible temperatures are lower (about 85 K at 300 Oe), but its dependence with temperature is stronger; *the increment of Sr has two consequences: an increment in the absolute value of the irreversibility temperature for a given field, and a weaker dependence of this temperature with the applied field.*

The described behavior can be understood in terms of Figs. 2 and 3: the initial dissipation is related, in the Sr doped samples, to the low temperature region, while, in the Sr free sample, it is provoked by the high temperature region of the curve, having the smallest value of slope (U) for a given field value. This implies that the intersect of this curve with the line that determines the voltage criterion (see Section 2.2) will be reached at a greater value of $1/T$ (i.e., smaller T). For the Sr doped samples, the greater is the Sr content, the greater is the slope in Fig. 2, so the smaller will be the intersect, being bigger the irreversibility temperature. Even for Sr17, the pinning energies (Fig. 3(a)) are bigger than those of Sr00 (Fig. 3(b)).

In Fig. 4(b) the irreversibility curves are shown in a more standard way. As can be seen in the legend, in parentheses, the power dependence of the irreversibility field with temperature becomes stepper as the Sr content increases, though again there is a jump for Sr20, for which the exponent is lower than that for Sr17. This behavior can be explained with the same philosophy of the previous paragraph: as can be seen in Fig. 3(a), the slope of U_1 vs. H for sample Sr20 is bigger than that of other doped samples, so as the field increases, the slope in the Arrhenius plot diminishes, having the consequence that the irreversibility temperature (i.e. the temperature of intersection of resistivity curve with the line of voltage criterion) will diminish faster with the field. It is worth noting how the intersection point of the curves for Sr20 and Sr28 in Fig. 3(a), is accounted in Fig. 4(b).

Regarding the position of the irreversibility line, the behavior is similar to that found for the field dependence of the pinning energy, i.e., the position of the irreversibility line is higher with the increment of Sr (as must be, according to all the previous reasoning). As we are dealing with intergranular properties, this result confirms the influence of the Sr content in the dissipation regimes of the transport currents. This effect can be related with two causes: the increment of the absolute value of irreversibility temperature with Sr content for a given field, and the decrement of T_{c0} (and $1 - T_z/T_{c0}$). The later statement means that, for a

given temperature T, the irreversibility field is bigger, the bigger is the Sr content. *So the Sr has beneficial effects not only over the intragranular irreversibility line, as has been reported before [6], but also for the intergranular one*. Regarding the slope, one can feel the temptation to affirm that the increment in the slope is disadvantageous for the intergranular region, being a problem when considering dissipation in ceramic superconducting polycrystals (as actually happens for intragranular irreversibility line). But it must be remembered the way the curves are measured: one fixes the magnetic field and increments the temperature, determining the onset of dissipation with a voltage criterion. So, in the present case, the increment in the slope means that the temperature of dissipation weakly depends on the applied magnetic field, which is very convenient for applications. The fact that sample Sr28 shows the best transport properties is puzzling, if you take a second look at Fig. 1(c): this sample shows in SEM a great porosity! It is an indication that the stacked grains form links whose conductivity weakly depends on the magnetic field, and probably dominate the overall transport properties.

Sr also influences the normal state resistivity: from Fig. 5, it can be seen that the general behavior described before is followed: the greater is Sr content, the lower is the normal state resistivity. This effect can be ascribed, firstly, to the decrease of the tensions in the crystal structure, due to the fact that, though both Sr and Ba have the same valence, Sr has smaller ionic radius than Ba. Secondly, the improvement in the connectivity between grains, and the increment in their size, also help in lowering normal state resistivity. It is also noticeable, in a closer look, that the onset critical temperature decreases with the Sr content, but the decrement is small, when compared with the decrement reported, for instance, in Ref. [6]. The values of T_{c0}, T_z, as well as the slope and intersect of the linear fit of normal state resistivity between 150 and 300 K ($\sigma_n = (a + bT)^{-1}$) are compared for the different Sr contents in Table 2. The measurement is precise enough to give a good estimate of the Varlamov–Livanov's temperature, so it gives a reasonable estimation of the normal state background.

From the data plotted in Fig. 6, and the onset critical temperature, the values of U_c were obtained (and presented in Table 2). It is easy to see that the interlayer coupling energy decreases with the increase of Sr in the sample. This is an indication of an increment in the interlayer distance. The effect that is usually obtained from the Sr–Ba substitution is the decrement of this distance, as a consequence of c-axis shrinking [7,16], associated to the so-called chemical pressure. According to [17] the simultaneous substitution of Ba by Sr and Hg by Re reduces the distance between the blocking layers (distance Cu–Hg–Cu), producing a reduction of the c-axis, as in our case, but the distance between the adjacent Cu planes (distance Cu–Cu) increases. One possible explanation of our situation is a partial substitution of Ca by Sr, due to the fact that the difference in ionic radius between Ba(IX) and Sr(IX) exceeds a little bit that between Sr(VIII) and Ca(VIII) [16]. In the present case for Sr17 there is not a clear indication of the occurrence of Ca–Sr substitution, because EDX analysis does not indicate deficiencies of Ba + Sr, and Ca content is approximately two. For Sr20 and Sr28 we find other relations: there is a concentration of Ba different than that required for the nominal stoichiometry, and there is also a deficit in Ca. So, the increment in coupling energy can be provoked by the partial Sr for Ca substitution. Another indication of this substitution is the decrement in the onset critical temperature with Sr content. In Ref. [16], a similar situation is explained by the possibility of Sr–Ca substitution, or a possible underdoping of their samples. Chmaissem et al. [17] also found a reduction on T_c, being related with structural changes associated with Re and Sr substitution. These substitution effects will be further studied in future work.

4. Conclusions

The resistive transition of (HgRe)-1223 superconducting polycrystals, in which Ba is partially substituted by Sr, indicates that Sr benefits transport properties, enhancing intergranular irreversibility line. In other words, the increment of Sr content, in the range under study, provokes that at

a given temperature, the field at which dissipation starts increments. The normal state resistivity decreases with the increment of Sr. However, the interlayer coupling energy, calculated from the fluctuation contribution to conductivity, indicates that the interlayer distance gets bigger with the Sr content. Our results suggest that Sr doping improves intergranular properties which can eventually decide the use of Hg-1223 polycrystals in transport applications.

Acknowledgements

Authors thank S. García for useful comments and discussion. A.J. Batista-Leyva and E. Altshuler thank R. Cruz (ICA1, Stuttgart) and J.A. Villanueva-Garibay (IPC, Stuttgart) for their help with correspondence. E. Altshuler thanks for the partial support from the World Laboratory Center for Pan-American Collaboration in Science and Technology. This work was partially supported by TWAS grant no. 95-124 RG/PHYS/LA and by the University of Havana's "Alma Mater" program.

References

[1] S.N. Putilin, E.V. Antipov, O. Chmaissen, M. Marezio, Nature 362 (1993) 226.
[2] A. Schilling, M. Cantoni, J.D. Guo, H.R. Ott, Nature 363 (1993) 56.
[3] J. Shimoyama, S. Hahakura, R. Kobayashi, K. Kitazawa, K. Yamafuji, K. Kishio, Physica C 235–240 (1994) 2795.
[4] K. Kishio, J. Shimoyama, A. Yoshikawa, K. Kitazawa, O. Chmaissen, J.D. Jorgensen, J. Low Temp. Phys. 105 (1996) 1359.
[5] A. Sin, A.G. Cunha, A. Calleja, M.T.D. Orlando, F.G. Emmerich, E. Baggio-Saitovich, M. Segarra, S. Piñol, X. Obradors, Adv. Mater. 10 (1998) 1226.
[6] S. Lee, N.P. Kiryakov, D.A. Emelyanov, M.S. Kuznetsov, Yu.D. Tetryakov, V.V. Petrykin, M. Kakihana, H. Yamauchi, Y. Zhuo, M.S. Kim, S.I. Lee, Physica C 305 (1998) 57.
[7] K. Yamaura, J. Shimoyama, S. Hahakura, Z. Hiroi, M. Takano, K. Kishio, Physica C 246 (1995) 351.
[8] L.E. Flores, C. Martínez, Cryogenics 36 (1996) 705.
[9] A.J. Batista-Leyva, R. Cobas, M.T.D. Orlando, C. Noda, E. Altshuler, Physica C 314 (1999) 73.
[10] A.J. Batista-Leyva, R. Cobas, E. Estévéz-Rams, M.T.D. Orlando, C. Noda, E. Altshuler, Physica C 331 (2000) 57.
[11] T. Henning, H. Kliem, A. Weyers, W. Bauhofer, Supercond. Sci. Technol. 10 (1997) 721.
[12] M. Auloos, Ch. Laurent, Phys. Rev. B 37 (1988) 611.
[13] H. Bougrine, M. Houssa, R. Cloots, M. Pekala, I. Sargankova, M. Ausloos, Supercond. Sci. Technol. 11 (1998) 128.
[14] A.A. Varlamov, D.V. Livanov, Sov. Phys. JETP 71 (1990) 325.
[15] E. Altshuler, C.W. Chu, A. Sin, M.T.D. Orlando, A.J. Batista-Leyva, V. Buntar, H.W. Weber, Physica C, accepted for publication.
[16] A. Sin, P. Odier, M. Núñez-Regueiro, M.T.D. Orlando, A.G. Cunha, Inst. Phys. Conf. Ser. No. 167 (2000) 283.
[17] O. Chmaissen, J.D. Jorgensen, K. Yamaura, Z. Hiroi, M. Takano, J. Shimoyama, K. Kishio, Phys. Rev. B 53 (1996) 14647.